

STUDY OF MASSIVE OBA STARS WITH X-RAY EMISSION

E. A. Nikolaeva^{1*}, I. F. Bikmaev^{1,2}, E. N. Irtuganov^{1,2}, M. R. Gilfanov^{3,4}, R. A. Sunyaev^{3,4},
P. S. Medvedev³

¹Kazan (Volga Region) Federal University, Kremlevskaya 18, Kazan 420008, Russia

²Tatarstan Academy of Sciences, Bauman 20, Kazan 420111, Russia

³Space Research Institute, Russian Academy of Sciences, Profsoyuznaya 84/32, 117997 Moscow, Russia

⁴Max Planck Institute for Astrophysics, Karl-Schwarzschild-Strasse 1, Garching bei München D-85741, Germany

A study of the physical parameters of a sample of 15 OBA-type stars with detected X-ray emission from the Spektr-RG/eROSITA telescope is presented. While X-ray emission from cool stars (spectral types F–G–K–M) originates in their near-surface regions, namely in the chromosphere and corona, the origin of X-ray emission in OBA stars requires case-by-case analysis since isolated OBA stars are not intrinsic X-ray emitters.

In this work, we derive the fundamental parameters of the stars in our sample, including the effective temperature T_{eff} and surface gravity $\log g$, based on spectral energy distribution fitting and optical spectroscopy obtained with the 1.5-m Russian–Turkish telescope RTT-150. An additional analysis of the $H\alpha$ line profiles allows us to identify possible mechanisms responsible for the observed X-ray emission, including non-stationary stellar winds, interactions in circumstellar material, and coronal emission from hidden cool companions.

We find that the X-ray emission in eight stars, with typical luminosities in the range $\log L_X = 28.5\text{--}30.0$, is most likely associated with hidden late-type companions.

Keywords: massive stars, X-ray emission, RTT-150, SRG/eROSITA

INTRODUCTION

Massive stars play a key role in the evolution of galaxies, acting as major sources of ionizing radiation, kinetic energy, and heavy elements. One of the primary manifestations of their activity is X-ray emission, the properties of which depend on the stellar spectral type. For the hottest stars (O-type), X-ray emission is mainly associated with shock waves in powerful radiatively driven winds, as well as with wind interactions in close binary systems. In B-type stars, the contribution from stellar winds becomes considerably weaker; instead, magnetic fields leading to the formation of magnetospheres, together with emission from hidden companions with active coronae, may dominate. A-type stars exhibit little to no intrinsic X-ray emission due to their weak winds and the absence of convective envelopes. Consequently, any detected emission from such objects is generally attributed to hidden late-type companions (Schröder & Schmitt, 2007) or, in some cases, to magnetic peculiarities.

X-ray emission in magnetic massive stars is commonly interpreted as arising from shock formation within magnetospheres, caused by collisions of stellar wind streams confined by magnetic fields. In these objects, the structure and dynamics of the stellar wind are largely governed by the magnetic field geometry. Flows emerging near the magnetic poles escape freely along open field lines into the interstellar medium, whereas at lower magnetic latitudes, charged particles are constrained to follow closed magnetic loops. As oppositely directed streams converge near the magnetic equator, they collide and form shock fronts. These regions produce hot plasma responsible for ultraviolet and X-ray emission in the surrounding region of the star (Babel & Montmerle, 1997a,b).

The launch of the *Spektr-RG* X-ray observatory (Sunyaev et al., 2021) with the *eROSITA* telescope (Predehl et al., 2020) on board, operating in the 0.3–10 keV range, has significantly expanded the capabilities for studying the X-ray properties of massive stars, providing wide sky coverage and high

* E-mail: evgeny.nikolaeva@gmail.com

sensitivity. At the same time, reliable interpretation of the X-ray data requires a comparison with the fundamental parameters of the stars themselves, which can be refined using modern photometric, astrometric, and spectroscopic measurements.

Photometric data for the selected objects were taken from the APASS DR9 (Henden & Munari, 2014), ASCC (Kharchenko, 2001), ALL-WISE (Wright et al., 2010), 2MASS (Skrutskie et al., 2006), SDSS DR12 (Alam et al., 2015), Pan-STARRS1 (Chambers et al., 2016), GALEX (Bianchi et al., 2011), Strömgren Photometric Catalog (Paunzen, 2015), GLIMPSE (Benjamin et al., 2003), Tycho-2 (Høg et al., 2000), and *Gaia* DR3 (Gaia Collaboration, 2023) catalogs, which provide broad coverage from the ultraviolet to the infrared. Astrometric parameters (parallaxes and proper motions) were taken from the *Gaia* mission, allowing us to refine the distances and select the nearest stars with the smallest uncertainties.

Spectroscopic data were obtained with the 1.5-m Russian-Turkish telescope RTT-150. The fundamental parameters of the stars in our sample were derived by fitting the observational data to model spectra and the spectral energy distribution (SED). The fitting process accounted for both the best match of the photometric data and SED to synthetic models and the detailed matching of diagnostic line profiles. For stars of spectral types B and A, the parameters were determined from the profiles of the hydrogen Balmer series lines; surface gravity was determined from the wings of these lines, which are most sensitive to this parameter. For O-type stars, the temperature was determined from the line ratios of helium in different ionization states, primarily He I $\lambda 4471$ and He II $\lambda 4541$, which serve as reliable indicators of the ionization balance in the atmosphere. The broadening of spectral lines due to rotation was accounted for using the projected rotational velocity $V \sin i$ values taken from the catalog of (Glebocki & Gnacinski, 2005).

Particular attention was paid to the H α line profile, which allows one to distinguish between the contribution of intrinsic processes in the stellar atmosphere, manifesting as emission components, and the presence of a possible hidden companion. Such companions have a well-developed convective envelope in which a dynamo mechanism operates, leading to intense magnetic activity. The heating of coronal plasma to temperatures of about 10^6 – 10^7 K as a result of magnetic reconnection and flaring processes produces their X-ray emission, characteristic of young stars of late spectral

types (F–M) (Wright et al., 2011). Typical X-ray luminosities for such objects are $\log L_X \sim 28.5$ – 30.0 (in erg s^{-1}) (Schröder & Schmitt, 2007; Güdel, 2004). According to (Schröder & Schmitt, 2007), if an A-type star is in a binary system with a late-type companion, the latter is generally a young, rapidly rotating star, leading to high magnetic activity and, accordingly, a significant level of X-ray emission. The rapid evolution of A-type stars compared to less massive late-type stars means that such companions remain relatively young and active at a stage when their more massive components have already evolved significantly.

THE SELECTION OF OBA STARS

The stellar sample was selected based on the criteria of belonging to hot stars in the upper part of the main sequence located within 3 kpc from the Sun:

1. Gaia absolute magnitude $M_G < 0.5$;
2. spectral classes A, B, O — i.e., stars without convective envelopes, chromospheres, and coronae, but exhibiting X-ray flux in the range $\log L_X = 28.5 - 31.5$. Known accreting close binary systems with compact companions (e.g., X Per) were excluded from the sample.

For the first group of stars targeted for spectroscopic observations with the RTT-150 telescope, 15 stars were selected; their initial parameters are given in Table 1.

The results of the X-ray flux measurements from the SRG/eROSITA surveys are given in Table 2.

OBSERVATIONS

The spectroscopic observations of the sample stars were carried out with the 1.5-m Russian–Turkish telescope (TUG, Antalya, Turkey) on 20–23 June 2025 using the TFOSC instrument in echelle mode. The spectra cover the wavelength range 3800–8800 Å at a medium spectral resolution of about 2.5 Å. Observations were performed with an Andor iKon-L 936 BEX2-DD-9ZQ CCD (2048×2048 pixels, $13.5 \mu\text{m}$ pixel size) cooled to -70°C , without binning. Two echelle exposures were obtained for each target, with exposure times between 600 and 1800 s depending on the stellar brightness. The spectra were reduced in the IRAF environment (Tody, 1986, 1993), including extraction of one-dimensional spectra, removal of cosmic rays and defects, continuum normalization, and wavelength calibration.

Table 1. Initial parameters of the stars

<i>N</i>	HD	RA	Dec	Gmag	Sp	π , mas	poe	$E(B - V)$	$(B - V)_0$	M_{G_0}	Fx	Fxerr	Fmax/Fmin
01	79158	09 13 48.21	+43 13 04.2	5.24	B9IV	5.27	33	0.00	-0.14	-1.13	5.07	1.20	—
02	112014	12 49 06.67	+83 25 04.2	5.83	A1IV	8.03	200	0.00	0.03	0.37	—	—	—
03	112028	12 49 13.73	+83 24 46.4	5.32	A1IVsh	7.77	67	0.00	-0.03	-0.22	9.85	1.02	2.03
04	118524	13 34 56.53	+70 07 08.4	7.50	A0e	2.94	22	0.00	0.04	-0.14	1.41	0.49	1.78
05	137569	15 26 20.81	+14 41 36.3	7.90	B9Ia	0.75	09	0.01	-0.05	-2.68	23.7	1.74	4.60
06	141458	15 48 50.48	+12 43 25.0	6.80	A0e	4.36	79	0.05	-0.02	-0.17	2.07	0.62	2.08
07	157087	17 20 09.83	+25 32 15.4	5.35	A3III	7.22	48	0.00	0.05	-0.35	2.80	0.65	3.21
08	157857	17 26 17.33	-10 59 34.8	7.71	O6eV	0.41	14	0.42	-0.31	-5.43	6.34	1.23	3.18
09	161693	17 43 59.16	+53 48 06.1	5.74	A2V	7.03	87	0.00	0.01	-0.02	3.64	—	1.32
10	161677	17 46 41.04	+05 46 27.4	7.10	B8e	2.88	93	0.16	-0.17	-1.09	7.57	1.31	2.10
11	164445	17 52 19.14	+76 00 02.4	7.29	F0e	3.11	162	0.09	0.25	-0.52	0.85	0.23	1.53
12	163800	17 58 57.25	-22 31 03.2	6.89	O7III	0.76	23	0.49	-0.25	-5.18	11.86	1.68	2.43
13	164438	18 01 52.28	-19 06 22.1	7.36	O9IV	0.82	29	0.55	-0.29	-4.78	9.11	1.47	5.18
14	174240	18 49 37.19	+00 50 10.3	6.22	A1IV	5.78	131	0.00	0.05	0.05	7.42	1.35	2.17
15	182422	19 23 46.92	+20 15 51.7	6.38	B9V	2.90	79	0.04	-0.02	-1.41	3.79	0.96	—

Notes. π , mas – parallax in milliarcseconds from Gaia DR3;

poe, i.e., the parallax-over-error, is the ratio of the Gaia DR3 parallax to its measurement error;

$E(B - V)$ – interstellar reddening. Derived from the 3D extinction maps of Green et al. (2019);

$(B - V)_0$ – dereddened $(B - V)$ color index;

M_{G_0} – dereddened absolute magnitude in the Gaia G -band. $M_{G_0} = G - 5 \log d + 5 - 1.25 A_G$. The extinction A_G is obtained from A_V using the conversion factor of 0.843 based on the extinction curves from Zhang et al. (2023), and an additional factor of 1.25 accounting for the temperature dependence of the $A_V \rightarrow A_G$ conversion (Fouesneau et al., 2023); the distance d from Bailer-Jones et al. (2021) was used for the calculations.

Fx(-14) – the mean X-ray flux in units of 10^{-14} erg s $^{-1}$ cm $^{-2}$ from the eROSITA telescope measurements in the 0.3–2.3 keV energy band;

Fmax/Fmin – the maximum-to-minimum flux ratio from the measurements in several eROSITA surveys (see Table 2).

METHOD DESCRIPTION

To determine the fundamental parameters of the stars, we used the astroARIADNE code (spectrAl eneRgy dIstribution bAyesian moDel averagiNg fittEr; (Vines & Jenkins, 2022)) based on fitting the spectral energy distribution (SED) and Bayesian model averaging over several stellar atmosphere models with weights proportional to their posterior likelihood. This approach accounts for the uncertainty associated with choosing a specific theoretical model and thus reduces systematic errors inherent in using a single grid of stellar atmosphere models.

The input data for the algorithm consist of broadband photometry corrected for interstellar extinction A_V derived from interstellar dust maps (Bayestar Green et al. (2019); dust maps Edenhofer et al. (2024) – added by us) and the Bailer-Jones distances (Bailer-Jones et al., 2021). The code interpolates theoretical grids of stellar atmosphere models over the parameters T_{eff} , $\log g$, and $[\text{Fe}/\text{H}]$, computing the likelihood

function by comparing observed and synthetic fluxes. Parameter estimation is performed via Markov chain Monte Carlo (MCMC) sampling, which efficiently explores the parameter space. The resulting posterior distributions provide the most probable parameter values and their confidence intervals. The stellar radius R_\star is obtained by scaling the model SED to the observed photometry using the distance; the bolometric luminosity L_{bol} follows from the Stefan–Boltzmann law; and the stellar mass M_\star is derived by interpolating the MIST evolutionary isochrones (Choi et al., 2016).

The astroARIADNE package uses the following theoretical stellar atmosphere grids: PHOENIX v2 (Husser et al., 2013), BT-Settl (Allard et al., 2012), BT-NextGen (Hauschildt et al., 1999; Allard et al., 2012), BT-Cond (Allard et al., 2012), Castelli & Kurucz (Castelli & Kurucz, 2003), Kurucz (Kurucz, 1993), and Coelho (Coelho, 2014).

To adapt the code for the study of massive stars, we additionally incorporated specialised atmosphere model grids designed for hot massive

Table 2. X-ray fluxes from the stars

<i>N</i>	HD	SRGe	e1	e1err	e2	e2err	e3	e3err	e4	e4err	e5	e5err	sens
01	79158	J091348.3+431307	—	—	—	—	—	—	—	—	—	—	1.13
02	112014	—	—	—	—	—	—	—	—	—	—	—	—
03	112028	J124913.2+832448	6.35	1.75	12.9	2.8	10.59	1.95	9.92	1.89	—	—	0.58
04	118524	J133454.6+700712	—	—	—	—	2.91	1.33	—	—	—	—	0.71
05	137569	J152620.9+144136	44.09	4.71	9.59	2.47	11.48	2.94	34.75	4.88	14.36	3.38	0.91
06	141458	J154850.6+124323	3.17	1.49	—	—	—	—	—	—	4.97	1.94	0.95
07	157087	J172009.6+253215	—	—	—	—	5.46	1.88	3.11	1.26	—	—	0.71
08	157857	J172617.3-105937	10.28	2.98	3.24	1.61	—	—	4.92	3.11	—	—	1.10
09	161693	J174359.2+534804	3.49	0.90	4.11	0.87	3.29	0.98	3.11	0.78	—	—	0.4
10	161677	J174641.1+054630	10.94	3.23	8.21	2.53	9.52	3.18	5.21	2.15	—	—	1.38
11	164445	J175218.9+760009	—	—	—	—	1.05	0.46	—	—	—	—	0.34
12	163800	J175857.4-223103	17.01	3.98	12.31	3.93	7.01	2.71	11.53	3.03	—	—	1.18
13	164438	J180152.5-190622	10.47	3.10	13.69	3.94	8.32	2.86	—	—	—	—	1.16
14	174240	J184937.1+005011	—	—	—	—	6.15	2.35	5.90	2.25	—	—	0.96
15	182422	J192346.8+201552	—	—	—	—	—	—	—	—	—	—	0.88

Notes. SRGe – the source number from the SRG/eROSITA catalog;

e1, e2, e3, e4, e5 – the fluxes in units of 10^{-14} erg s $^{-1}$ cm $^{-2}$ registered in surveys 1–5;

e1err, e2err, e3err, e4err, e5err – the flux errors in units of 10^{-14} erg s $^{-1}$ cm $^{-2}$ in the corresponding surveys;

sens – the sensitivity in units of 10^{-14} erg s $^{-1}$ cm $^{-2}$ in the total accumulation for the sky region near the corresponding X-ray source.

stars ($T_{\text{eff}} > 15\,000$ K): PoWR (Pauli et al., 2025; Hainich et al., 2019), TLUSTY (Werner & Dreizler, 1999; Rauch & Deetjen, 2003; Werner et al., 2003), and TMAP (Hubeny & Lanz, 1995; Lanz & Hubeny, 2003, 2007).

The output of the code is illustrated for the star 36 Lyn in the following figures:

- the corner diagram showing the posterior distributions of the physical parameters (Fig. 1),
- the spectral energy distribution fitted with the most probable (highest-likelihood) theoretical atmosphere model (Fig. 2),
- the position of the best-fitting parameters on the Hertzsprung–Russell diagram (Fig. 3), and
- the posterior samples of T_{eff} and $\log g$ with individual model probabilities, and the averaged posterior samples (Fig. 4).

The parameters derived for all stars are listed in Table 3. A detailed discussion of the obtained parameters, including an analysis of the possible presence of hidden companions and the origin of X-ray emission for individual stars, is presented in the following sections.

THE NATURE OF THE X-RAY EMISSION FROM INDIVIDUAL SOURCES

36 Lyn (=HD 79158)

36 Lyn is a bright ($V = 5.28^m$), well-studied, chemically peculiar magnetic star of late B type (B8p) with weak helium lines. Wade et al. (2006) performed a comprehensive analysis using polarimetric and spectroscopic observations. They derived the stellar parameters ($T_{\text{eff}} \approx 13\,000$ – $13\,600$ K, $\log g \approx 3.7$ – 4.2 , $\log L/L_{\odot} = 2.54 \pm 0.16$, $R_{\star} = 3.4 \pm 0.7 R_{\odot}$, $B_p = 3.57 \pm 0.36$ kG), confirmed the variability of the H α line core profile due to the occultation of the core by circumstellar gas, and interpreted the spread in radial velocity measurements ranging from $+21$ km s $^{-1}$ (Hoffleit & Warren, 1991) to 29.7 ± 1.6 km s $^{-1}$ (Takada-Hidai & Aikman, 1989) as being due to the variability of the metal line profiles caused by their nonuniform distribution on the stellar surface and the variability of the H α line profile due to the presence of circumstellar gas. During our spectroscopic observations, the star was at a phase where the emission component in the H α line was absent (Fig. 5).

According to Berghoefer et al. (1996), the star 36 Lyn was not reliably detected by the ROSAT

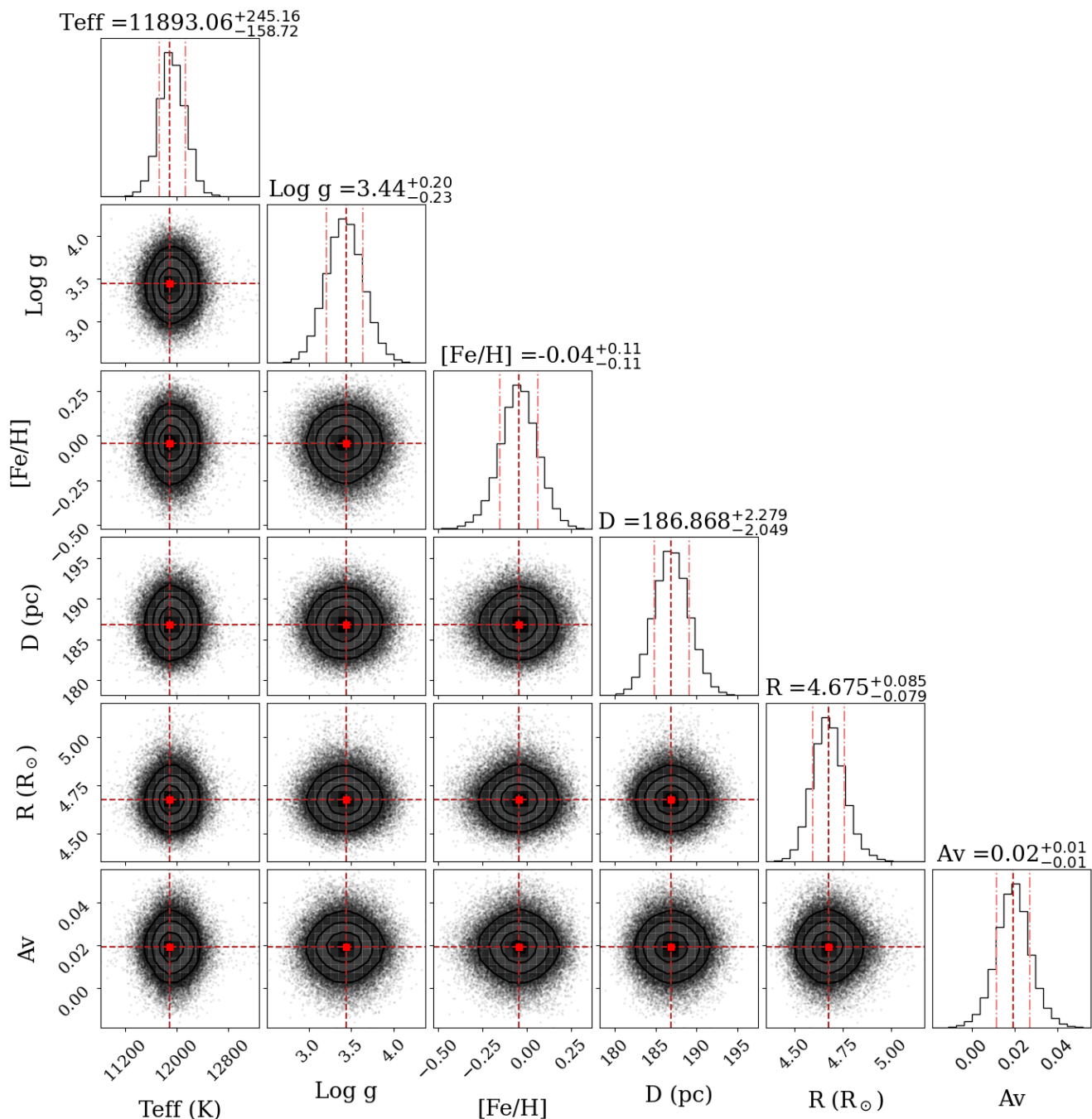


Fig. 1. Corner plot showing the posterior distributions of the physical parameters for the star 36 Lyn.

X-ray observatory, and only an upper limit on its X-ray luminosity was given: $\log L_X < 29.84$. The SRG/eROSITA X-ray telescope detected X-ray emission from the star with $\log L_X = 29.33$, which is slightly below that upper limit. There are two possible explanations for the origin of the X-ray emission in the system:

1. Heating of material and generation of X-rays in closed magnetic loops formed by the interaction of the magnetic field with the stellar wind;
2. The X-ray emission originates from a companion – an F0 star discovered by speckle interferometry (Balega et al., 2012).

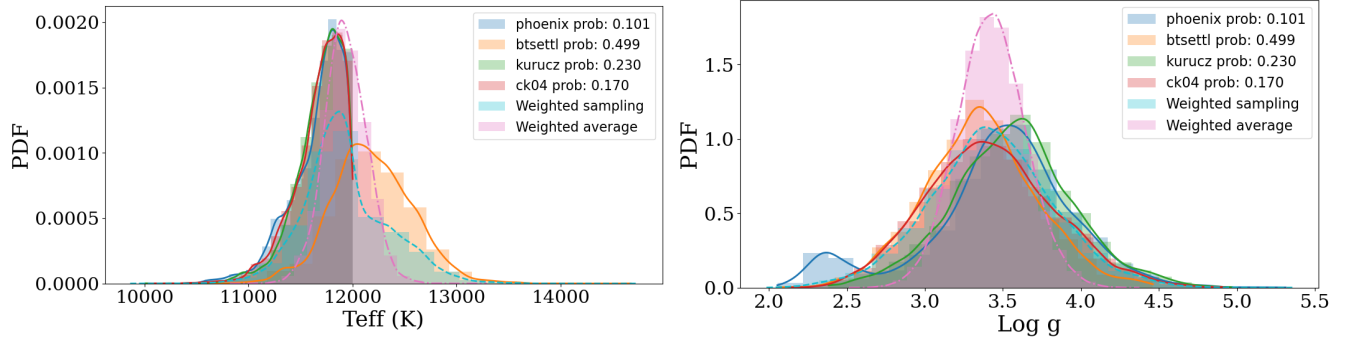


Fig. 4. The posterior distributions of T_{eff} and $\log g$ for 36 Lyn. The samples from the posterior distributions obtained with astroARIADNE for different model grids are shown. The posterior probability is indicated for each model.

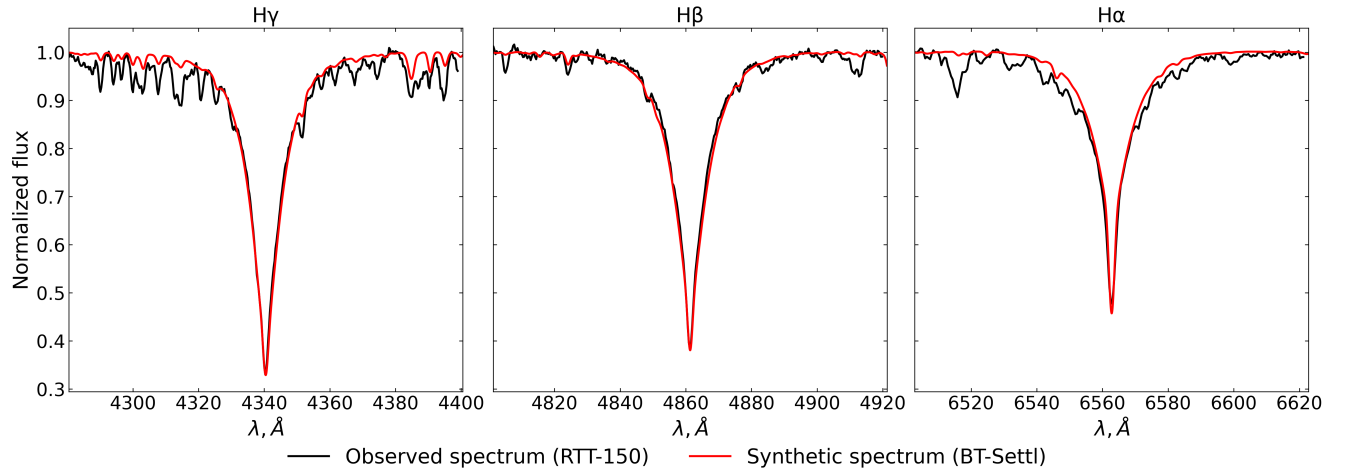


Fig. 5. Comparison of the observed and theoretical spectra (based on the BT-Settl model) for the star 36 Lyn.

+ A2 V, that orbit their common centre of mass with a period of $P_{\text{orb}} \sim 3.3$ d on a nearly circular orbit ($e \approx 0.04$) (Eggleton & Tokovinin, 2008). In our spectra, lines of only one component are present.

According to the Schröder & Schmitt catalog of A stars with hidden companions (Schröder & Schmitt, 2007), HD 112028 is included among the detected “bona fide” single A-type stars reliably associated with X-ray sources ($\log L_X = 29.01$), strongly suggesting the presence of a hidden late-type companion. HD 112014, by contrast, appears among the X-ray associated A-type stars that are members of known binary or multiple systems or show signs of hidden companions, with an X-ray luminosity of $\log L_X = 28.63$.

New measurements with the SRG/eROSITA telescope have made it possible to unambiguously establish that the X-ray source is the star HD 112028, given the positional accuracy of the

X-ray coordinates of $5''$. At the position of the star HD 112014, no X-ray flux is detected at the sensitivity level of 5.83×10^{-15} erg s $^{-1}$ cm $^{-2}$.

The X-ray luminosity of HD 112028 measured by SRG/eROSITA is $\log L_X = 29.29$. Such a level of X-ray emission is typical of late-type hidden companions. Moreover, the spectrum of HD 112028 exhibits no signatures of peculiarity or a magnetic field that would explain such X-ray luminosity. Consequently, HD 112028 is at least a binary system, whereas the double star HD 112014 is not the source of the X-ray emission.

HD 118524

HD 118524 is an ordinary A-type star. The X-ray luminosity detected by the SRG/eROSITA telescope is $\log L_X < 29.29$ and indicates the presence of a hidden companion. According to *Gaia* data, the $RUWE = 4.75$ value significantly exceeds the threshold $RUWE_{\text{threshold}} = 1.23$ (Castro-

Table 3. Parameters of the stars

Star	d_{BJ} (pc)	T_{eff} (K)	$\log g$ (dex)	R_{\star} (R_{\odot})	Age (10^6 yr)	M_{\star} (M_{\odot})	L_{bol} (L_{\odot})	$\log L_{\text{X}}$ **	$\log L_{\text{X}}$ (CPI)	$\log\left(\frac{L_{\text{X}}}{L_{\text{bol}}}\right)$	Comp.
36 Lyn	188_{-5}^{+5}	11893_{-281}^{+380}	$3.4_{-0.4}^{+0.3}$	$4.7_{-0.1}^{+0.1}$	161_{-25}^{+86}	$3.5_{-0.1}^{+0.6}$	396_{-45}^{+54}	< 29.84	29.33	-6.85	✓?
HD 112014	$124.2_{-0.5}^{+0.6}$	9630_{-172}^{+203}	$3.9_{-0.3}^{+0.3}$	$3.0_{-0.1}^{+0.1}$	430_{-100}^{+134}	$2.5_{-0.3}^{+0.2}$	69_{-6}^{+7}	28.63 ?			
HD 112028	128_{-2}^{+2}	9983_{-89}^{+81}	$3.6_{-0.2}^{+0.2}$	$5.5_{-0.1}^{+0.1}$	240_{-25}^{+37}	$3.6_{-0.2}^{+0.2}$	275_{-18}^{+16}	29.01	29.29		✓
HD 118524	338_{-13}^{+15}	8839_{-165}^{+168}	$3.5_{-0.3}^{+0.3}$	$2.3_{-0.1}^{+0.1}$	731_{-129}^{+480}	$2.0_{-0.4}^{+0.1}$	30_{-3}^{+3}		29.29		✓
HD 137569	1288_{-134}^{+140}	11989 ***	2.00 ***	43_{-15}^{+5}	88_{-8}^{+8}	$5.3_{-0.2}^{+0.2}$	33988_{-19748}^{+7314}	31.21	31.67	-6.44	
HD 141458	228_{-2}^{+3}	9036_{-192}^{+283}	$3.4_{-0.3}^{+0.3}$	$3.9_{-0.1}^{+0.1}$	574_{-57}^{+44}	$2.3_{-0.1}^{+0.1}$	92_{-10}^{+12}		29.11		✓
HD 157087	138_{-3}^{+3}	8488_{-136}^{+178}	$3.4_{-0.2}^{+0.2}$	$4.8_{-0.1}^{+0.1}$	419_{-36}^{+118}	$2.9_{-0.3}^{+0.1}$	110_{-10}^{+11}		28.81		✓
HD 161677	341_{-3}^{+3}	14804_{-1206}^{+489}	$3.7_{-0.2}^{+0.2}$	$3.8_{-0.1}^{+0.2}$	122_{-43}^{+33}	$4.2_{-0.3}^{+0.5}$	619_{-177}^{+131}		30.02	-6.35	
HD 161693	142_{-2}^{+1}	9043_{-162}^{+199}	$3.4_{-0.2}^{+0.2}$	$3.9_{-0.1}^{+0.1}$	580_{-135}^{+40}	$2.3_{-0.1}^{+0.3}$	92_{-8}^{+10}	29.32 ?	28.94		✓
HD 164445	319_{-2}^{+2}	6909_{-71}^{+67}	$3.4_{-0.4}^{+0.4}$	$6.7_{-0.1}^{+0.2}$	549_{-36}^{+25}	$2.5_{-0.1}^{+0.1}$	93_{-5}^{+6}		29.01	-6.54	
HD 174240	172_{-1}^{+1}	8942_{-214}^{+192}	$3.6_{-0.1}^{+0.1}$	$3.9_{-0.1}^{+0.1}$	456_{-48}^{+80}	$2.6_{-0.3}^{+0.2}$	87_{-8}^{+9}	29.34	29.42		✓
HD 182422	340_{-5}^{+4}	9362_{-311}^{+360}	$2.9_{-0.2}^{+0.2}$	$7.1_{-0.2}^{+0.2}$	234_{-25}^{+31}	$3.5_{-0.2}^{+0.2}$	346_{-47}^{+60}	< 29.55	29.72		✓
HD 157857	2272_{-163}^{+145}	36094_{-916}^{+916}	$3.8_{-0.5}^{+0.3}$	$13.4_{-1.1}^{+1.3}$	4_{-1}^{+1}	$27.4_{-2.9}^{+5.4}$	270692_{-47981}^{+66973}	< 32.76*	31.59	-7.42	
HD 163800	1250_{-45}^{+55}	34629_{-1317}^{+1403}	$3.7_{-0.1}^{+0.1}$	$11.1_{-0.6}^{+0.6}$	4_{-2}^{+3}	$23.0_{-3.8}^{+4.5}$	159374_{-29155}^{+33043}		31.35	-7.44	
HD 164438	1166_{-30}^{+32}	31977_{-774}^{+580}	$3.8_{-0.2}^{+0.1}$	$10.2_{-0.6}^{+0.7}$	4_{-3}^{+2}	$18.3_{-1.5}^{+1.8}$	96747_{-14869}^{+16356}		31.17	-7.40	

Notes. d_{BJ} – the Bailer-Jones distance (Bailer-Jones et al., 2021).

* The logarithm of X-ray luminosity obtained from the Einstein observatory data (Chlebowski et al., 1989).

** The logarithm of X-ray luminosity obtained from the ROSAT observatory data (Schröder & Schmitt, 2007). The question mark denotes the stars from the list of A-type stars in binary or multiple systems associated with the X-ray emission for which there is evidence of hidden companions.

*** The value was derived from the spectroscopic data and fixed when fitting the SED fitting, because the spectral energy distribution did not allow reliable determination of the parameter due to a significant contribution from infrared radiation caused by the presence of a disk in the system.

In the last column, the symbol “✓” indicates the presence of a hidden companion in the system.

Ginard et al., 2024), further supports the existence of a secondary component.

HD 137569

HD 137569 is a binary star located at a high Galactic latitude and belongs to the old Galactic population. Orbital parameters of the system are known from the 9th Catalogue of Spectroscopic Binary Orbits (Pourbaix et al., 2004): orbital period $P_{\text{orb}} = 529.8$ d, eccentricity $e = 0.11$, and radial-velocity semi-amplitude $K_1 = 15.8$ km s $^{-1}$. The primary star of the binary system is in the post-asymptotic giant branch (post-AGB) stage and has an extremely low metallicity $[\text{Fe}/\text{H}] = -3$ (Kluska et al., 2022).

The binary system is surrounded by a gas-dust disk (Kluska et al., 2022), whose emission manifests as a slight infrared excess and an emission contribution in the H α line and partially in the H β line (Fig. 7). The ROSAT satellite detected emission with a hardness ratio $\text{HR} = -1$, indicating

very soft X-rays, and a flux $F_{\text{X}} = 8.12 \times 10^{-14}$ erg s $^{-1}$ cm $^{-2}$ (Freund et al., 2022). The flux measured by the SRG/eROSITA telescope is $F_{\text{X}} = 2.37 \times 10^{-13}$ erg s $^{-1}$ cm $^{-2}$, corresponding to an X-ray luminosity of $\log L_{\text{X}} = 31.7$.

The pronounced underabundance of metals detected in the stellar atmosphere can be interpreted as evidence of re-accretion of gas depleted in dust from the circumbinary disk onto the post-AGB star (Oomen et al., 2019), since heavy elements preferentially condense onto dust grains in the circumbinary disk. The combination of a soft X-ray component ($\log L_{\text{X}} > 31$, $\text{HR} = -1$) and the filled H α profile suggests that this process likely continues at the present time, manifesting itself as low-efficiency accretion of residual gaseous disk material.

HD 141458

The HD 141458 system is a well-studied spectroscopic binary. Its orbital elements were first

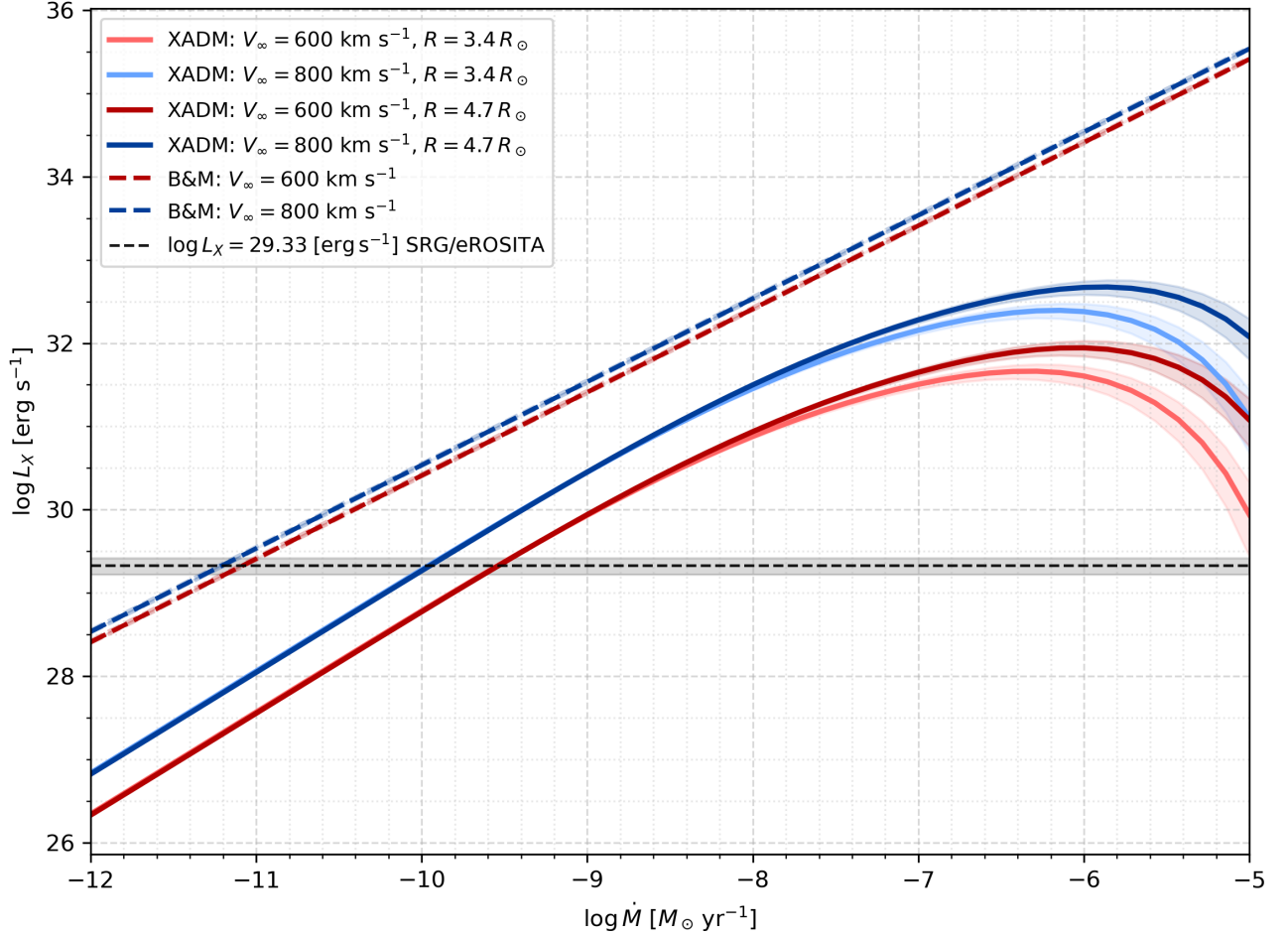


Fig. 6. Calculated X-ray luminosity as a function of mass-loss rate using the analytic formula of the XADM model (X-ray Analytic Dynamical Magnetosphere, (ud-Doula et al., 2014)) – solid line, and the power-law relation of Babel & Montmerle (1997a) – dashed line for several sets of parameters V_∞ and R_* . The magnetic field strength is taken to be $B = 3.57 \pm 0.36$ kG (Wade et al., 2006). The radius value $R_* = 3.4R_\odot$ is taken from (Wade et al., 2006), while $R_* = 4.7R_\odot$ is obtained in the present work. As can be seen from the plot, the model curves derived for different radii begin to diverge noticeably only at large values of \dot{M} , whereas in the region of the observed X-ray luminosity these differences are practically absent. The transparent area illustrates the uncertainty range.

determined by Bolton et al. (1983), who derived radial velocity curves for both components and obtained a full orbital solution. The system has an orbital period of $P = 28.949$ d and a significant eccentricity of $e = 0.64$. The semi-amplitudes of the radial velocity curves are $K_1 = 60.6$ km s $^{-1}$ and $K_2 = 66.6$ km s $^{-1}$, corresponding to a mass ratio close to unity, $m_1/m_2 = 1.1$.

Both stars belong to spectral class A: the primary is classified as A0V and the secondary as A1V. In our spectra, only the A1V component is reliably detected. The orbital parameters derived by Bolton et al. were later confirmed and included in the 9th Catalogue of Spectroscopic Binary Orbits (SB9;

Pourbaix et al., 2004). Horch et al. (2017) measured a separation between the components of $0.4923''$ using speckle interferometry, with a magnitude difference of 3.5 mag.

The X-ray luminosity measured by SRG/eROSITA is $L_X = 1.29 \times 10^{29}$ erg s $^{-1}$. Since both visible components are A-type stars and therefore cannot be X-ray sources, the most probable explanation is a hidden late-type companion whose emission is produced by an active corona.

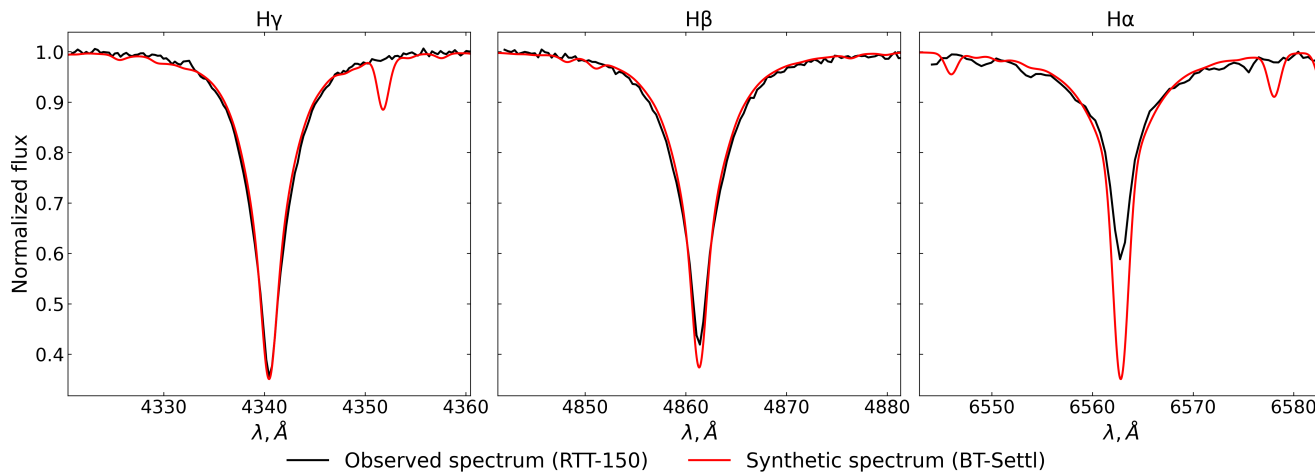


Fig. 7. Comparison of the observed and synthetic spectra ((based on the BT-Settl model) for HD 137569.

HD 157087

HD 157087 was studied in detail by Khalack (2018), who refuted its classification as an Am star (Yüce et al., 2011; Preston, 1974; Adelman, 1987). The observed features include the variability of the mean abundances of some chemical elements against an almost constant background of the others, a significant enhancement of C, S, Ca, Sc, V, Cr, Mn, Co, Ni, and Zr with depth in the atmospheric layers, and overabundances of Ca and Sc. The author interprets all of these as evidence that the star is chemically peculiar, with characteristics close to those of Am stars but exhibiting pronounced vertical stratification.

Analysis of radial velocity measurements revealed both long-period and short-period variations. The long-period variations support the suggestion that HD 157087 is an astrometric binary with a period exceeding 6 yr (Makarov & Kaplan, 2005). The presence of short-period radial velocity variations, together with temporal changes in the mean chemical abundances, indicates that HD 157087 may be a triple system in which a short-period binary orbits a third star. In this case, the short-period pair may consist of two slowly rotating stars of spectral types Am and A (or a weakly magnetic Ap star), with similar effective temperatures and $\log g$ values but different chemical peculiarities.

The SRG/eROSITA X-ray data likewise point to the multiplicity of the system. Its X-ray luminosity $L_X = 6.39 \times 10^{28} \text{ erg s}^{-1}$ stems from a hidden low-mass companion, as no magnetic field is detected in the system (Khalack, 2018). The fundamental parameters we derive for the system fully agree with

those reported by Khalack (2018) ($T_{\text{eff}} = 8882 \text{ K}$, $\log g = 3.57$) and correspond to a star of spectral type A3 III.

HD 161677

HD 161677 is a rapidly rotating single B5V star with a projected rotational velocity of $V \sin i = 210 \text{ km s}^{-1}$ (Glebocki & Gnacinski, 2005) and a rotation period of $P_{\text{rot}} = 0.233 \text{ d}$ (Fig. 8). It is a member of the small, young open cluster IC 4665 (Negueruela et al., 2024).

The cluster was observed with the ROSAT satellite (Giampapa et al., 1998); however, no X-ray emission from HD 161677 was detected. According to SRG/eROSITA observations, the X-ray luminosity of the star is $\log L_X = 30.02$.

As in other rapidly rotating B-type stars in the cluster, the X-ray emission of HD 161677 is produced by shock heating in a radiatively driven stellar wind. Inhomogeneous gas flows interact, giving rise to shocks with temperatures of several million kelvin, which generate soft X-ray emission.

HD 161693 (=Alruha)

HD 161693 is a normal main-sequence A1 star (Zorec & Royer, 2012) and shows no intrinsic properties that could account for detectable X-ray emission. Nevertheless, in the catalog of X-ray A stars in binary and multiple systems (Schröder & Schmitt, 2007), based on ROSAT data, the star was classified as a candidate object with a hidden companion.

In this catalogue, HD 161693 is given an X-ray luminosity of $L_X = 2.08 \times 10^{29} \text{ erg s}^{-1}$, comparable

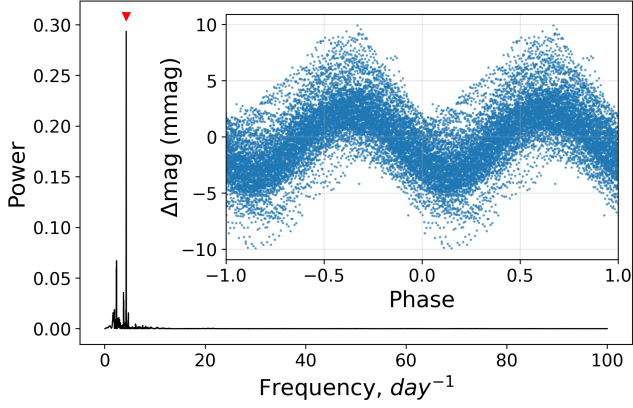


Fig. 8. Periodogram and phase-folded light curve of HD 161677 based on TESS data (Sector 80). The main panel shows the Lomb–Scargle periodogram (Lomb, 1976; Scargle, 1982), with the dominant period $P_{\text{rot}} = 0.233$ d. The inset displays the phase-folded light curve using this period. The fluxes are converted into relative magnitudes.

to the SRG/eROSITA estimate of ($L_X = 0.88 \times 10^{29}$ erg s $^{-1}$).

The SRG/eROSITA observations, benefiting from higher astrometric accuracy, allow a secure identification of the X-ray source with HD 161693. This supports the interpretation that the X-ray emission originates from a hidden low-mass companion.

HD 164445

We classify this object as an F2V star with a projected rotational velocity of $V \sin i = 120$ km s $^{-1}$. According to *Gaia* astrometry, the renormalised unit weight error, $\text{RUWE} = 1.121$, is below the sky-varying threshold of $\text{RUWE}_{\text{threshold}} = 1.229$ defined in Castro-Ginard et al. (2024), and therefore shows no evidence of an astrometric signature of a hidden companion.

Early F-type stars possess relatively shallow convective envelopes, which limit the efficiency of the magnetic dynamo and typically result in low levels of coronal activity. At the same time, the high rotational velocity of the star ($V \sin i = 120$ km s $^{-1}$) implies a small Rossby number, making the dynamo more efficient and thereby enhancing both magnetic activity and X-ray emission.

According to Wright et al. (2011), F-type stars do not exhibit a well-defined saturation regime: as the Rossby number decreases, their coronal activity passes straight from the supersaturated to the unsaturated regime without forming an extended plateau.

Given the above, the observed X-ray luminosity of this object, $L_X = 1.03 \times 10^{29}$ erg s $^{-1}$, is most likely driven by a combination of its relatively rapid rotation and a still-operating, though weakened, magnetic dynamo in a thin convective envelope.

HD 174240

The star HD 174240 has been included in several high-quality spectral libraries. The *HST Low-Resolution Stellar Library* (LOWLIB) (Pal et al., 2023) provides a STIS spectrum covering 0.2–1.0 μm , with an Mg II $\lambda 2800$ index of 0.194 mag, indicative of photospheric absorption and a lack of pronounced chromospheric activity. The stellar parameters derived from this library are $T_{\text{eff}} = 8879$ K, $\log g = 3.61$, and $[\text{Fe}/\text{H}] = -0.63$, corresponding to spectral type A1 IV. The *X-shooter Spectral Library* (XSL) (Verro et al., 2022) reports the following parameter estimates: $T_{\text{eff}} = 9262$ K, $\log g = 3.65$, and $[\text{Fe}/\text{H}] = -0.4$ (Arentsen et al., 2019).

Measurements of the magnetic field of HD 174240 are compiled in two catalogues. The *FORS1 catalogue of stellar magnetic field measurements* (Bagnulo et al., 2015) includes a series of FORS1/ESO VLT observations that yielded no significant detection ($\langle B_z \rangle < 50$ G, below the 2σ level). A *catalogue and statistical analysis of magnetic stars* (Rustem et al., 2023) yields a root-mean-square magnetic field of approximately 79 ± 76 G, based on ~ 4 measurements. These values are inconsistent with the strong, stable fields characteristic of Ap/Bp stars and therefore do not indicate intrinsic magnetically driven coronal activity.

X-ray emission from HD 174240 was detected in the *ROSAT All-Sky Survey* (Schröder & Schmitt, 2007; Schröder et al., 2008), with a luminosity of $\log L_X \approx 29.3$ erg s $^{-1}$. The authors interpreted this signal as originating from a hidden late-type companion. According to SRG/eROSITA observations, the X-ray luminosity of the star amounts to $\log L_X \approx 29.43$ erg s $^{-1}$.

Thus, the combination of spectral properties, the low Mg II $\lambda 2800$ index, the absence of an intrinsic magnetic field, and the presence of X-ray emission indicates that HD 174240 does not exhibit intrinsic chromospheric or coronal activity. The observed X-ray emission is instead attributed to a low-mass, late-type companion.

HD 182422

HD 182422 is classified as a star of spectral type A1V. Our derived effective temperature of

$T_{\text{eff}} = 9362$ K is in good agreement with the value $T_{\text{eff}} = 9772$ K reported in the PASTEL catalogue (Soubiran et al., 2016). The *Gaia* astrometric quality indicator $\text{RUWE} = 1.135$ does not exceed the sky-dependent threshold $\text{RUWE}_{\text{threshold}} = 1.218$, providing no evidence for significant astrometric binarity (Castro-Ginard et al., 2024).

The *ROSAT All-Sky Survey* provides an upper limit on the X-ray luminosity of HD 182422 is $\log L_X < 29.55$ erg s $^{-1}$ (Berghoefer et al., 1996), while SRG/eROSITA observations yield $\log L_X = 29.72$ erg s $^{-1}$, which may indicate the presence of a hidden companion.

O-type stars

HD 157857, HD 163800, and HD 164438 have been classified within the Galactic O-Star Spectroscopic Survey (GOSSS; Sota et al. 2011, 2014) as O6.5 II(f), O7.5 III((f)), and O9.2 IV stars, respectively. Martins et al. (2005) provides calibrations of stellar parameters for Galactic O-type stars across different luminosity classes. Figures 9 and 10 show the best-fitting PoWR models computed using the stellar parameters derived with the astroARIADNE code. The models reproduce the hydrogen, helium, and Si III lines observed in HD 157857. The effective temperatures derived in the present work are in good agreement with those expected from the spectral classifications and the calibrations of Martins et al. (2005), who employed the CMFGEN code, while the surface gravities are systematically higher, which may be attributed to the use of different stellar atmosphere codes (CMFGEN and PoWR).

A weak longitudinal magnetic field of $\langle B_z \rangle = -110 \pm 46$ G, measured using all available spectral lines, has been detected in HD 157857 (Hubrig et al., 2013). Weak H α emission is present in the spectrum (Fig. 9), indicating the presence of a stellar wind and possibly weak magnetospheric activity. Based on data from the *Einstein* X-ray Observatory (Chlebowski et al., 1989), only an upper limit on the X-ray luminosity of $\log L_X < 32.76$ could be derived for this star.

HD 163800 is a typical representative of late O7–O8 giants with a moderately strong radiatively driven stellar wind. Its spectrum shows N III $\lambda\lambda 4634$ – 4642 and He II $\lambda 4686$ emission features, characteristic of the ((f)) classification and attributed to recombination emission in the stellar wind.

HD 164438 is a spectroscopic binary system consisting of an O9.2 subgiant and a B5 main-sequence companion (Blex et al., 2024). The orbital

period of the system is 10.2 d. The H α line shows emission filling, suggesting a small but non-negligible contribution from the stellar wind.

According to SRG/eROSITA data, all three stars have X-ray luminosities on the order of $\log L_X \approx 31.5$, consistent with standard shock-heating processes in unstable radiatively driven stellar winds (Feldmeier et al., 1997).

STARS WITH HIDDEN COMPANIONS. DISCUSSION

To investigate the origin of the X-ray emission, we derived the fundamental parameters of 15 OBA-type stars with X-ray luminosities in the range $\log L_X = 28.5$ – 31.5 , based on SRG/eROSITA data. We find that the X-ray emission of five OB-type stars originates either in circumstellar envelopes or in collisional processes within stellar magnetospheres. The presence of stellar winds is supported by the observed composite H α line profiles, which consist of photospheric absorption combined with emission in the line core produced by the wind component in the circumstellar environment. In eight A-type stars, the H α line profiles are well described by photospheric absorption alone. Moreover, available studies indicate that these stars do not host strong global magnetic fields. Consequently, the X-ray emission in these eight objects is attributed to the coronae of hidden cool companions—late-type dwarf stars.

We identify the presence of hidden companions in two stars from the list of “bona fide” systems presented by Schröder & Schmitt (2007). In the second probabilistic list of binary candidates, one system is confirmed while another is rejected.

For 36 Lyn, the presence of a hidden companion is firmly established, and the companion is classified as an F0 V star. For objects of this type, the typical bolometric luminosity is $\log L_{\text{bol}} = 0.89$ (Pecaut & Mamajek, 2013). The resulting ratio $\log(L_X/L_{\text{bol}}) = -5.14$ is consistent with the unsaturated regime of coronal activity typical of F0 V stars. Nevertheless, the possibility that the X-ray emission originates from magnetic activity of the primary star itself cannot be entirely excluded.

For HD 182422, we derive an age of approximately 234 Myr. The hidden companion is likely of comparable age and therefore belongs to the population of young late-type stars (G–M) that still reside in the saturated regime of coronal activity, for which $\log(L_X/L_{\text{bol}}) \approx -3$. Adopting this value allows us to estimate the bolometric luminosity of the companion and hence its spectral

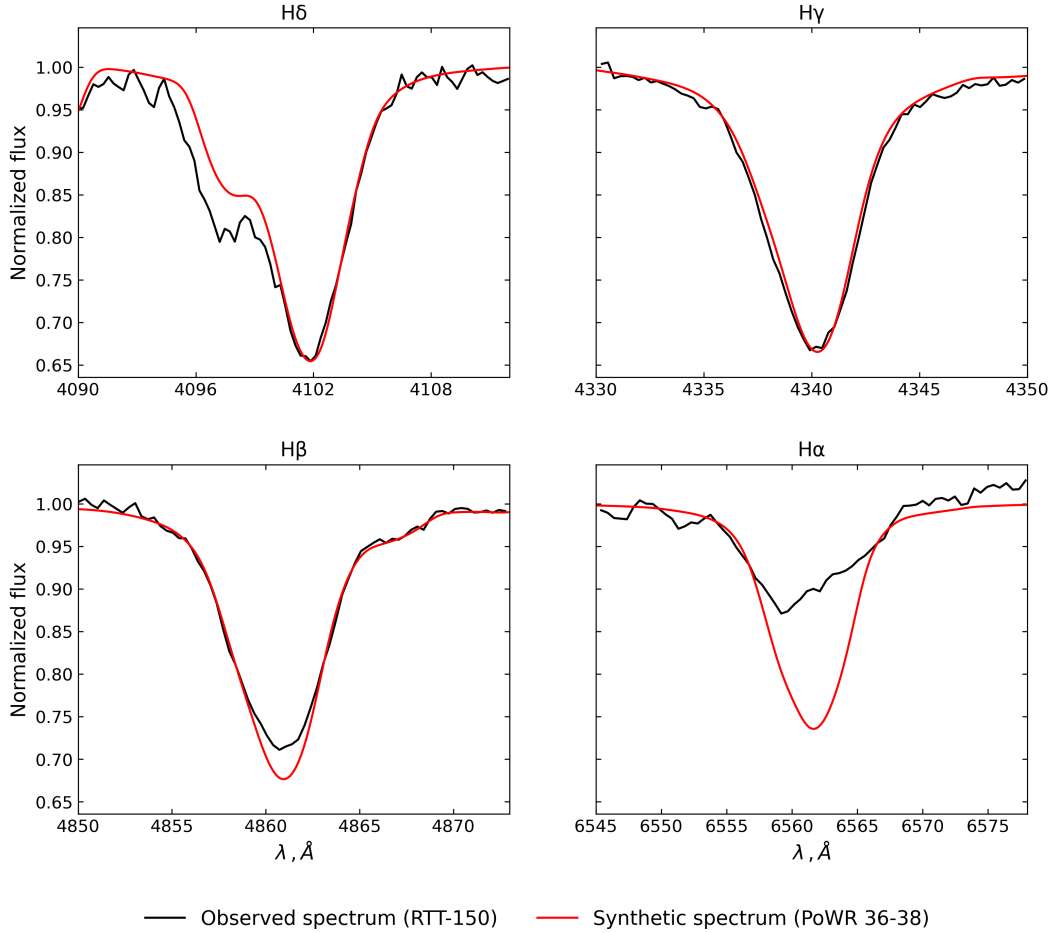


Fig. 9. Observed spectrum of HD 157857 compared with a PoWR synthetic spectrum ($T_{\text{eff}} = 36\,000\text{ K}$, $\log g = 3.8$), which provides the best fit to the observed data.

type. The derived value corresponds to a late-type star of approximately K5 V–K7 V.

For the remaining stars the spectral type of the hidden companion may range from F to M. The range $\log(L_X/L_{\text{bol}}) \sim -3$ to -5 , characteristic of coronally active stars, translates into bolometric luminosities consistent with spectral types from M dwarfs to F-type stars. As illustrated in Fig. 12 of Johnstone et al. (2021), at $L_X \sim 10^{29}\text{ erg s}^{-1}$ the allowed mass range spans this entire interval, making an unambiguous determination of the spectral type not possible.

ACKNOWLEDGMENTS

This study is based on observations with the eROSITA telescope onboard the SRG observatory. The SRG observatory was built by Roskosmos in the interests of the Russian Academy of Sciences represented by the Space Research Institute (IKI) within the framework of the Russian Federal Space

Program, with the participation of the Deutsches Zentrum für Luft- und Raumfahrt (DLR). The SRG/eROSITA X-ray telescope was built by a consortium of German institutes led by MPE, and supported by DLR. The SRG spacecraft was designed, built, launched, and is operated by the Lavochkin Association and its subcontractors. The science data are downlinked via the Deep Space Network Antennae in Bear Lakes, Ussurijsk, and Baykonur, funded by Roskosmos. The eROSITA data used in this paper were processed with the eSASS software developed by the German eROSITA consortium and the software developed by the Russian SRG/eROSITA consortium.

This work has made use of data from the European Space Agency (ESA) mission *Gaia* (<https://www.cosmos.esa.int/gaia>), processed and analyzed by the Gaia DPAC consortium (<https://www.cosmos.esa.int/web/gaia/dpac/>

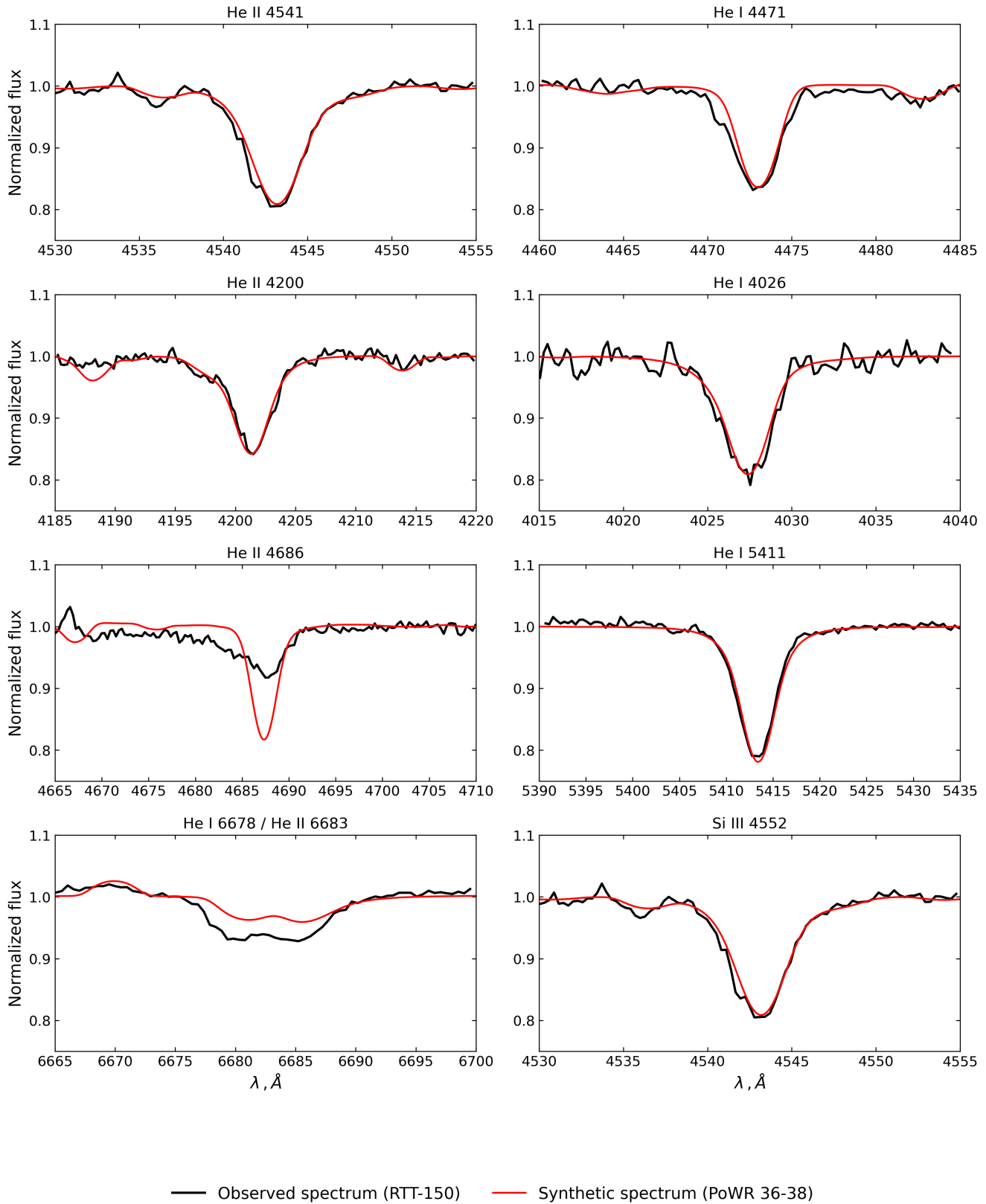


Fig. 10. Comparison of the PoWR model with the He I, He II, and Si III lines of HD 157857 (cf. Fig. 9).

consortium).

E.A. Nikolaeva thanks the “Summer School for Astrostatistics in Crete - 2024” for training on the statistical methods used in this paper.

FUNDING

We are grateful to TUBITAK, the Space Research Institute, the Kazan Federal University, and the Academy of Sciences of Tatarstan for their partial support in using RTT-150 (the 1.5-m Russian–Turkish telescope in Antalya).

The work of E.A. Nikolaeva, I.F. Bikmaev, and E.N. Irtuganov was supported by subsidy FZSM-2023-0015 of the Ministry of Education and Science of the Russian Federation granted to the Kazan Federal University for the State assignment in the sphere of scientific activities.

REFERENCES

1. S.J. Adelman, *Astron. Astrophys. Suppl. Ser.* **67**, 353 (1987).
2. S. Alam, F.D. Albareti, C. Allende Prieto, et al., *Astrophys. J. Suppl. Ser.* **219**, id12 (2015).
3. F. Allard, D. Homeier, and B. Freytag, *Philosophical Transactions of the Royal Society of London Ser. A* **370**, 2765 (2012).
4. Y. Andriillat, M. Jäschek, C. Jäschek, et al., *Astron. Astrophys. Suppl. Ser.* **65**, 1 (1986).
5. A. Arentsen, P. Prugniel, A. Gonneau, et al., *Astron. Astrophys.* **627**, A138 (2019).
6. M. Babel and T. Montmerle, *Astron. Astrophys.* **323**, 121 (1997a).
7. J. Babel and T. Montmerle, *Astrophys. J.* **485**, L29 (1997b).
8. S. Bagnulo, J.D. Landstreet, L. Fossati, et al., *Astron. Astrophys.* **583**, A115 (2015).
9. C.A.L. Bailer-Jones, J. Rybizki, M. Foesneau, et al., *Astron. J.* **161**, 147 (2021).
10. Yu.Yu. Balega, V.V. Dyachenko, A.F. Maksimov, и др., *Astrophys. Bull.* **67**, 44 (2012).
11. R.A. Benjamin, E. Churchwell, B.L. Babler, et al., *Publ. Astron. Soc. Pacific* **115**, 953 (2003).
12. T.W. Berghoefter, J.H.M.M. Schmitt, and J.P. Cassinelli, *Astron. Astrophys. Suppl. Ser.* **118**, 481 (1996).
13. L. Bianchi, Y.B. Kang, B. Efremova, et al., *Astrophys. Space Sci.* **335**, 161 (2011).
14. S. Blex, M. Haas, R. Chini, et al., *Astron. Astrophys.* **692**, A192 (2024).
15. C.T. Bolton, M. Bates, and R. Hurkens, *JRASC* **77**, 18 (1983).
16. F. Castelli and R.L. Kurucz, *Proceed. of the 210th Symp. of the Inter. Astronomical Union held at Uppsala University* (Ed. N. Piskunov, W.W. Weiss, and D.F. Gray, Uppsala: Astron. Soc. Pacific, 2003), A20 (2003).
17. A. Castro-Ginard, Z. Penoyre, A.R. Casey, et al., *Astron. Astrophys.* **688**, A1 (2024).
18. K.C. Chambers, E.A. Magnier, N. Metcalfe, et al., *arXiv*, 1612.05560 (2016).
19. T. Chlebowski, F.R. Harnden, and S. Sciortino, *Astrophys. J.* **341**, 427 (1989).
20. J. Choi, A. Dotter, C. Conroy, et al., *Astrophys. J.* **823**, 102 (2016).
21. P.R.T. Coelho, *MNRAS* **440**, 1027 (2014).
22. A. ud-Doula and S.P. Owocki, *Astrophys. J.* **576**, 413 (2002).
23. A. ud-Doula, S. Owocki, R. Townsend, et al., *MNRAS* **441**, 3600 (2014).
24. G. Edenhofer, C. Zucker, P. Frank, et al., *Astron. Astrophys.* **685**, A82 (2024).
25. P.P. Eggleton and A.A. Tokovinin, *MNRAS* **389**, 869 (2008).
26. A. Feldmeier, J. Puls, and A.W.A. Pauldrach, *Astron. Astrophys.* **322**, 878 (1997).
27. M. Foesneau, Y. Frémat, R. Andrae, et al., *Astron. Astrophys.* **674**, A28 (2023).
28. S. Freund, S. Czesla, J. Roßbrade, et al., *Astron. Astrophys.* **664**, A105 (2022).
29. Gaia Collaboration (Gaia Collaboration, A. Vallenari, A.G.A. Brown, et al.), *Astron. Astrophys.* **674**, A1 (2023).
30. M.S. Giampapa, C.F. Prosser, and T.A. Fleming, *Astrophys. J.* **501**, 624 (1998).
31. R. Glebocki and P. Gnaniński, 13th Cambridge Workshop on Cool Stars, Stellar Systems and the Sun **560**, 571 (2005).
32. G.M. Green, E. Schlafly, C. Zucker, et al., *Astrophys. J.* **887**, 93 (2019).
33. M. Güdel, *Astron. Astrophys. Rev.* **12**, 71 (2004).
34. R. Hainich, V. Ramachandran, T. Shenar, et al., *Astron. Astrophys.* **621**, A85 (2019).
35. P.H. Hauschildt, F. Allard, and E. Baron, *Astrophys. J.* **525**, 871 (1999).
36. A. Henden and U. Munari, *CAOSP* **43**, 518 (2014).
37. D. Hoffleit and W.H.Jr. Warren, *New Haven*, (1991).
38. E. Høg, C. Fabricius, V.V. Makarov, et al., *Astron. Astrophys.* **355**, L27 (2000).
39. E.P. Horch, D.I. Casetti-Dinescu, M.A. Camarata, et al., *Astron. J.* **153**, 212 (2017).
40. I. Hubeny and T. Lanz, *Astrophys. J.* **439**, 875 (1995).
41. S. Hubrig, M. Schöller, I. Ilyin, et al., *Astron. Astrophys.* **551**, A33 (2013).
42. T.-O. Husser, S. Wende-von Berg, S. Dreizler, et al., *Astron. Astrophys.* **553**, A6 (2013).

43. C.P. Johnstone, M. Bartel, M. Güdel, et al., *Astron. Astrophys.* **649**, A96 (2021).
44. V. Khalack, *MNRAS* **477**, 882 (2018).
45. N.V. Kharchenko, *Kinematika Fiz. Nebesn. Tel* **17**, 409 (2001).
46. J. Kluska, H. Van Winckel, Q. Coppée, et al., *Astron. Astrophys.* **658**, A36 (2022).
47. R. Kurucz, ATLAS9 Stellar Atmosphere Programs and 2 km/s grid, Smithsonian Astrophysical Observatory, Kurucz CD-ROM No. 13, (1993).
48. T. Lanz and I. Hubeny, *Astrophys. J. Suppl. Ser.* **146**, 417 (2003).
49. T. Lanz and I. Hubeny, *Astrophys. J. Suppl. Ser.* **169**, 83 (2007).
50. N.R. Lomb, *Astrophys. Space Sci.* **39**, 447 (1976).
51. V.V. Makarov and G.H. Kaplan, *Astron. J.* **129**, 2420 (2005).
52. F. Martins, D. Schaerer, and D.J. Hillier, *Astron. Astrophys.* **436**, 1049 (2005).
53. I. Negueruela, S. Simón-Díaz, A. de Burgos, et al., *Astron. Astrophys.* **690**, A176 (2024).
54. G. Oomen, H. Van Winckel, O. Pols, et al., *Astron. Astrophys.* **629**, A49 (2019).
55. T. Pal, I. Khan, G. Worthey, et al., *Astrophys. J. Suppl. Ser.* **266**, 41 (2023).
56. D. Pauli, L.M. Oskinova, W.-R. Hamann, et al., *Astron. Astrophys.* **697**, A114 (2025).
57. E. Paunzen, *Astron. Astrophys.* **580**, A23 (2015).
58. M.J. Pecaut and E.E. Mamajek, *Astrophys. J. Suppl. Ser.* **208**, 9 (2013).
59. D. Pourbaix, A.A. Tokovinin, A.H. Batten, et al., *Astron. Astrophys.* **424**, 727 (2004).
60. P. Predehl, R. Andritschke, V. Arefiev, et al., *Astron. Astrophys.* **647**, A1 (2021).
61. G.W. Preston, *Ann. Rev. Astron. Astrophys.* **12**, 257 (1974).
62. T. Rauch and J.L. Deetjen, *Stellar Atmosphere Modeling, ASP Conf. Proc.* (Ed. I. Hubeny, D. Mihalas, K. Werner, San Francisco: Astron. Soc. Pacific) **103**, (2003).
63. A. Rustem, Guo-Liang Lü, Chun-Hua Zhu, et al., *Res. Astron. Astrophys.* **23**, id095024 (2023).
64. J.D. Scargle, *Astrophys. J.* **263**, 835 (1982).
65. C. Schröder and J.H.M.M. Schmitt, *Astron. Astrophys.* **475**, 677 (2007).
66. C. Schröder, S. Hubrig, and J.H.M.M. Schmitt, *Astron. Astrophys.* **484**, 479 (2008).
67. M.F. Skrutskie, R.M. Cutri, R. Stiening, et al., *Astron. J.* **131**, 1163 (2006).
68. A. Sota, J. Maíz Apellániz, N.R. Walborn, et al., *Astrophys. J. Suppl. Ser.* **193**, 24 (2011).
69. A. Sota, J. Maíz Apellániz, N.I. Morrell, et al., *Astrophys. J. Suppl. Ser.* **211**, 10 (2014).
70. C. Soubiran, J.-F. Le Campion, N. Brouillet, et al., *Astron. Astrophys.* **591**, A118 (2016).
71. R. Sunyaev, V. Arefiev, V. Babyshkin, et al., *Astron. Astrophys.* **656**, A132 (2021).
72. M. Takada-Hidai and G.C.L. Aikman, *Publ. Astron. Soc. Pacific* **101**, 699 (1989).
73. D. Tody, *Instrumentation in astronomy VI* **627**, 733 (1986).
74. D. Tody, *Astronomical Data Analysis Software and Systems II* **52**, 173 (1993).
75. K. Verro, S.C. Trager, R.F. Peletier, et al., *Astron. Astrophys.* **660**, A34 (2022).
76. J.I. Vines and J.S. Jenkins, *MNRAS* **513**, 2719 (2022).
77. G.A. Wade, M.A. Smith, D.A. Bohlender, et al., *Astron. Astrophys.* **458**, 569 (2006).
78. K. Werner and S. Dreizler, *J. Comput. Appl. Math.* **109**, 65 (1999).
79. K. Werner, J.L. Deetjen, S. Dreizler, et al., *Stellar Atmosphere Modeling, ASP Conf. Proc.* (I. Hubeny, D. Mihalas, K. Werner, San Francisco: Astron. Soc. Pacific) **31**, (2003).
80. E.L. Wright, P.R.M. Eisenhardt, A.K. Mainzer, et al., *Astron. J.* **140**, 1868 (2010).
81. N.J. Wright, J.J. Drake, E.E. Mamajek, et al., *Astrophys. J.* **743**, 48 (2011).
82. K. Yüce, S.J. Adelman, A.F. Gulliver, et al., *Astron. Nachr.* **332**, 681 (2011).
83. X. Zhang, G.M. Green, and H. Rix, *MNRAS* **524**, 1855 (2023).
84. J. Zorec and F. Royer, *Astron. Astrophys.* **537**, A120 (2012).